Letter

Shaping magnetic order by local frustration for itinerant fermions on a graph

Revathy B. S.[*] and Shovan Dutta[†]
Raman Research Institute, Bangalore 560080, India

(Received 15 July 2025; revised 3 June 2026; accepted 12 June 2026; published 22 July 2026)

Kinetic magnetism is an iconic and rare example of collective quantum order that emerges from the interference of paths taken by a hole in a sea of strongly interacting fermions. Here, the lattice topology plays a fundamental role, with odd loops frustrating ferromagnetism, as seen in recent experiments. However, the resulting magnetic order on a general graph has remained elusive. Here, we systematically establish a general principle: that local frustration centers bind singlets while sharing a delocalized hole. This collective effect—absent in exchange magnetism—extends from rectangular grids to random graphs, producing sharp and predictable variation with tunable frustration measures. Our findings demonstrate that one can shape the spin order and tune the net magnetization by embedding kinetic frustration, opening ways of spatially resolved quantum control of many-body systems. We outline a protocol to realize some of the key findings in existing cold-atom setups.

DOI: 10.1103/stj9-srp1

Introduction. Frustrated magnetism is a classic setting in which the lattice topology dictates collective ordering, giving rise to strongly correlated phases of matter such as spin liquids and spin ice [1–3]. In the more commonly studied case, frustration arises from competing spin-exchange interactions defined on the bonds of a lattice, which cannot all be simultaneously satisfied [4]. A distinct type of frustration arises from destructive quantum interference of paths taken by mobile spins, which increases the kinetic energy for certain spin configurations [5,6]. Unlike exchange coupling, this kinetic magnetism has no classical counterpart. How such a purely quantum-mechanical order is governed by the loop structure of the lattice is a fundamental question that has remained elusive for several decades.

Both exchange and kinetic magnetism are found in the Hubbard model [7–9] which, in the limit of strong on-site repulsion, describes hopping of spin-$\uparrow$ and spin-$\downarrow$ fermions along with an antiferromagnetic spin exchange. The hopping is suppressed when each site has one spin (half-filling) but dominates in the presence of a hole. Every hop by the hole rearranges the spins and changes the sign of the wave function. Thus, moving the hole around a loop with an even number of sides gives a constructive interference if the spins are aligned. This effect makes the ground state ferromagnetic on generic bipartite lattices, as was shown by Nagaoka [10]. In contrast, an odd loop frustrates this order [5], favoring a singlet (spin zero) ground state for one triangle [11]. For extended regular lattices with frustration, the ordering varies with geometry—while a triangular lattice gives rise to a 120° classical antiferromagnet [5,12], special corner-sharing geometries such as a triangular cactus [11] or a pyrochlore lattice [13,14] can stabilize a spin liquid of singlets. Recent experiments have supported these findings on a square plaquette [15] and a triangular lattice [16,17]. However, the path interferences are considerably more complex on a general graph, where both even and odd loops exist side by side. While one expects the ferromagnetic state to be destabilized [12,18–20], there is no understanding of the resulting magnetic order, despite the possibility of realizing such connectivities in optical traps [21–23] or with qubit encodings [24–26].

This is also a fundamental question from the point of view of network science [27,28], where a principal finding of a growing number of studies is that network structure can radically alter collective phenomena such as disease spreading, percolation, and synchronization [29–31]. However, these findings are limited to classical systems, with rare exceptions [32–35]. In particular, studies of frustration have focused on social balance [36] and Ising spin-glass physics [30].

Here, we explore the impact of local frustration on kinetic magnetism using a bottom-up approach. By adding frustration centers (diagonal bonds) to a rectangular grid one at a time, we establish that they locally bind singlets while preserving delocalization of the hole and the spin-polarized background, which allows one to shape the spin ordering as well as tune the net magnetization in steps of 1 by embedding frustration (Fig. 4). Moreover, this strong, collective effect extends to random graphs, where the magnetization is anticorrelated with different measures of local frustration and exhibits a characteristic oscillation as a function of the smallest loop size (Fig. 5). Such prominent variation is in stark contrast with exchange magnetism at half-filling, where both the total spin [34] and the local spin alignment show a lack of sensitivity to frustration; see Supplemental Material (SM) [37].

Setup. We consider the Hubbard Hamiltonian [9,38]

$$\hat{H} = -\sum_{\langle i,j\rangle,\sigma} t_{i,j}(\hat{c}^\dagger_{i\sigma}\hat{c}_{j\sigma} + \hat{c}^\dagger_{j\sigma}\hat{c}_{i\sigma}) + U\sum_i \hat{n}_{i\uparrow}\hat{n}_{i\downarrow}, \quad (1)$$

[*]Contact author: revathy1bs@gmail.com
[†]Contact author: shovan.dutta@rri.res.in

where the first term describes hopping of a fermion with spin $\sigma \in \{\uparrow, \downarrow\}$ between neighboring sites i and j with amplitude $t_{i,j} > 0$ (for $t_{i,j} < 0$, ferromagnetism is not frustrated [39–41]), and the second term describes on-site interaction between fermions of opposite spin, with occupations $\hat{n}_{i\sigma} := \hat{c}^\dagger_{i\sigma}\hat{c}_{i\sigma}$. To focus on the role of network structure on kinetic magnetism, we study the limit of one hole and $U \to \infty$. The latter suppresses double occupancies so the physics is governed solely by the kinetic energy of the hole. We define on-site spin operators $\hat{S}^z_i := \frac{1}{2}(\hat{n}_{i\uparrow} - \hat{n}_{i\downarrow})$, $\hat{S}^+_i := \hat{c}^\dagger_{i\uparrow}\hat{c}_{i\downarrow}$, and $\hat{S}^-_i := \hat{c}^\dagger_{i\downarrow}\hat{c}_{i\uparrow}$ and collective spin operators $\hat{S}^z = \sum_i \hat{S}^z_i$ and $\hat{S}^\pm = \sum_i \hat{S}^\pm_i$. The net magnetization, measured by $\hat{S}^2 = (\hat{S}^z)^2 + \frac{1}{2}(\hat{S}^+\hat{S}^- + \hat{S}^-\hat{S}^+)$, has eigenvalues of the form $S_{\rm total}(S_{\rm total}+1)$ with $S_{\rm total} \in \{N/2, N/2-1, \ldots, N/2 - \lfloor N/2 \rfloor\}$, where N is the total number of fermions. The Hubbard Hamiltonian has a global rotational symmetry [8,9] such that each energy eigenstate has a definite $S_{\rm total}$ and a degeneracy of $2S_{\rm total}+1$, which corresponds to different numbers of $\downarrow$ spins, $N_\downarrow \in [N/2 - S_{\rm total}, N/2 + S_{\rm total}]$. It is thus sufficient to compare the lowest energies for $N_\downarrow = N/2 - S_{\rm total} \in [0, N/2]$ to find the ground-state magnetic order.

Square with diagonal bonds. We start by analyzing a single square with hopping t along the sides and t' across the diagonals [Fig. 1(a)]. The square has reflection symmetry about the x and y axes, leading to four parity sectors $\{(+,+), (+,-), (-,+), (-,-)\}$, of which $(+,-)$ and $(-,+)$ have the same energies. For $t' = 0$, the ground state is a Nagaoka ferromagnet [15].

To study the effect of frustration, we set $t' = 1 - t = u$ and plot the minimum energy sector as a function of u in Fig. 1(b). For $N_\downarrow = 0$, the ground state is just that of a hole hopping with amplitudes $-t$ and $-t'$, given by $|\psi\rangle = \frac{1}{2}(\hat{c}_{1\uparrow} - \hat{c}_{2\uparrow} - \hat{c}_{3\uparrow} + \hat{c}_{4\uparrow})|{\uparrow\uparrow\uparrow\uparrow}\rangle$ for $t' < t$. This state is represented in Fig. 1(c), where the dotted bonds are frustrated and the alternating signs indicate the π quasimomentum. The state has energy $E = -2t + t'$ and remains the ground state for $u < \frac{1}{5}$, beyond which the square binds a singlet, requiring $N_\downarrow = 1$. Here, the system can take 12 different configurations $(i,j) \equiv \hat{S}^-_j \hat{c}_{i\uparrow}|{\uparrow\uparrow\uparrow\uparrow}\rangle$, where i denotes the position of the hole and j denotes that of the $\downarrow$ spin (magnon). The problem then becomes that of a single particle hopping on a 12-site Hilbert-space graph shown in Figs. 1(d) and 1(e). For $t' > t$, the frustration is minimized by the configuration in Fig. 1(e), which describes the state

$$|{\times}\rangle_\uparrow = [(\hat{S}^-_1 - \hat{S}^-_4)(\hat{c}_{2\uparrow} - \hat{c}_{3\uparrow}) - (\hat{S}^-_2 - \hat{S}^-_3)(\hat{c}_{1\uparrow} - \hat{c}_{4\uparrow})]|{\uparrow\uparrow\uparrow\uparrow}\rangle,$$

corresponding to a singlet on one diagonal and an $\uparrow$-spin hopping on the other diagonal [inset of Fig. 1(b)], leading to diagonal singlet correlations [Fig. 1(h)]. This "cross-dimer" state with $(-,-)$ parity has energy $E = -t - t'$ and is the ground state for $u > \frac{1}{2}$. For $\frac{1}{5} < u < \frac{1}{2}$, the ground state varies with u, with $E = -\sqrt{3t^2 + t'^2}/(t + t')$ and $(\pm,\mp)$ parity. The one with $(-,+)$ parity is sketched in Fig. 1(d) and has the form $|\psi\rangle = |{\mid\mid}\rangle + x\,|{=}\rangle$, where

$$|{\mid\mid}\rangle = [(\hat{S}^-_1 - \hat{S}^-_2)(\hat{c}_{3\uparrow} - \hat{c}_{4\uparrow}) - (\hat{S}^-_3 - \hat{S}^-_4)(\hat{c}_{1\uparrow} - \hat{c}_{2\uparrow})]|{\uparrow\uparrow\uparrow\uparrow}\rangle,$$

$$|{=}\rangle = [(\hat{S}^-_1 - \hat{S}^-_3)(\hat{c}_{2\uparrow} + \hat{c}_{4\uparrow}) + (\hat{S}^-_2 - \hat{S}^-_4)(\hat{c}_{1\uparrow} + \hat{c}_{3\uparrow})]|{\uparrow\uparrow\uparrow\uparrow}\rangle,$$

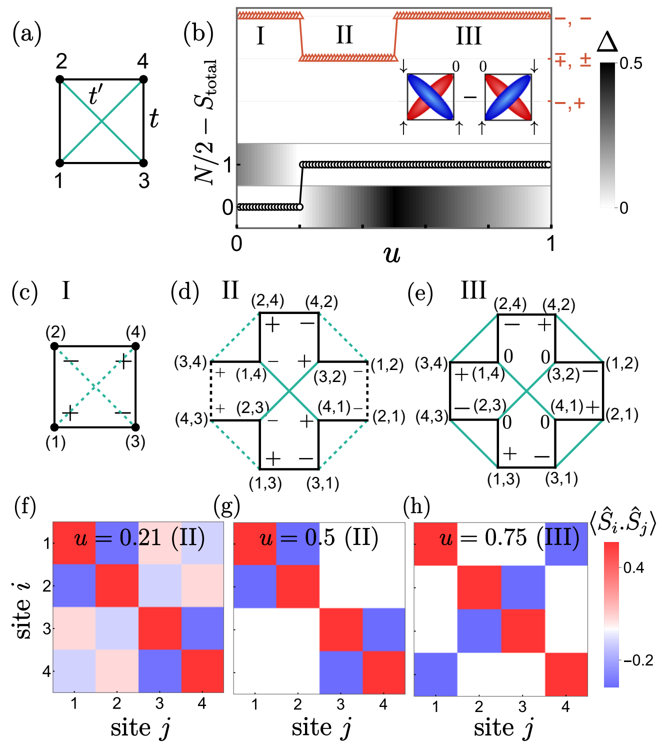

FIG. 1. (a) Square with tunneling $t = 1 - u$ along the sides (black) and $t' = u$ on the diagonals (green), containing $N = 3$ fermions with total spin $S_{\rm total} \in \{1/2, 3/2\}$. (b) Magnetization (circles) and reflection parity (triangles) of the ground state as a function of u. The spin gap Δ (minimum energy gap from the ground-state sector) is plotted in the background. The inset shows a "cross-dimer" structure of the ground state in region III, where blue and red ellipses denote a singlet and a delocalized hole, respectively. (c)–(e) Hilbert-space graph representation of the ground state. The vertices correspond to the position of the hole in I and those of the hole and the $\downarrow$ spin (magnon) in II and III. The signs indicate the relative amplitudes of the wave function and dashed lines show frustrated edges. (f)–(h) Spin correlations showing antialigned spins on the vertical bonds in II and on the diagonal bonds in III.

and x increases from 0 to $\frac{1}{5}$ as u decreases from $\frac{1}{2}$ to $\frac{1}{5}$. The $|{\mid\mid}\rangle$ component gives rise to singlet correlations on the vertical bonds, as shown in Figs. 1(f) and 1(g).

Ladder with a frustrated plaquette. Next, we embed a frustrated square at the center of a ladder [Fig. 2(a)]. From exact diagonalization, there are again three regions, except that $S_{\rm total}$ is reduced by 2 in region III [Fig. 2(b)]. Surprisingly, the magnons are always strongly bound to the frustrated plaquette [Fig. 2(d)], even when the hole is delocalized for $u \lesssim \frac{1}{2}$ [Fig. 2(c)]. This is consistent with an effective attraction between the hole and magnons in the presence of frustration [42]. The ordering is similar to that of the single square, with singlet correlations on the vertical rungs in region II and on the diagonals in region III. Due to the strong binding, the physics is unaltered by increasing the length l of the ladder.

The small spread in the magnon density outside the central plaquette in region III [Fig. 2(d)] can be understood from perturbation theory in t/t'. Here, the hole is bound to the central plaquette, and to first order, the perturbation selects

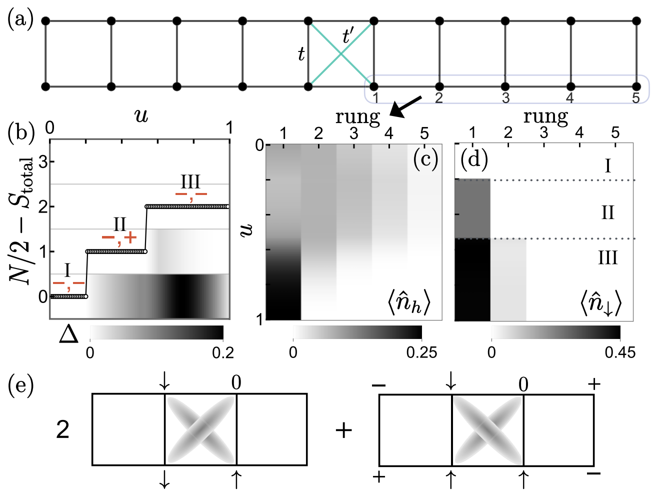

FIG. 2. (a) Ladder with a central frustrated plaquette. (b) Minimum energy sector and ground-state parity as a function of $u = t' = 1 - t$, with the excitation gap Δ plotted in the background. (c) Hole density $\langle \hat{n}_h \rangle$ and (d) $\downarrow$-spin density $\langle \hat{n}_\downarrow \rangle$, showing that the magnons are strongly bound to the center even when the hole is not. (e) Sketch of the cross-dimer–type ground state for large u. The results are for a ladder of length $l = 10$; however, they do not change for $l \gtrsim 4$.

two types of cross-dimer states with $(-,-)$ parity: (i) $|\times\rangle_\downarrow$, where the hole hops with a $\downarrow$ spin across a diagonal, and (ii) $|\times\rangle_{\uparrow,d}$, where the hole hops with an $\uparrow$ spin across a diagonal, and the second $\downarrow$ spin is at a distance $d \in \{1, 2, 3, \dots\}$ from the central plaquette. To lift this degeneracy, the hole has to make three hops along a neighboring plaquette, which couples $|\times\rangle_\downarrow$ and $|\times\rangle_{\uparrow,1}$, selecting the ground state $2|\times\rangle_\downarrow + |\times\rangle_{\uparrow,1}$, as sketched in Fig. 2(e). Hence, the probability of finding a magnon outside the central plaquette is $P_{\text{out}} = \frac{1}{5}$. Note this perturbative estimate remains valid throughout region III [Fig. 2(d)]. We also show in Appendix A that the physics is similar for a square grid with x-y symmetry and a frustrated central plaquette. Here, the magnons for large t' are even more strongly bound with $P_{\text{out}} = \frac{1}{9}$.

In contrast, for Heisenberg antiferromagnetism at half-filling, $S_{\text{total}} = 0$ for all u and the spin alignment across the diagonal bonds varies smoothly with u (see SM [37]).

Ladder with two frustrated plaquettes. We next model a ladder with two frustrated squares embedded symmetrically at a distance p from the center [Fig. 3(a)]. When p is sufficiently small, the hole mediates interactions between the two, producing strong collective effects.

The phase diagram for large l shows five different regions [Fig. 3(b)]. Two of these can be understood from the physics of the single frustrated plaquette: In region II, the hole is delocalized and each frustrated plaquette binds one $\downarrow$ spin, with singlet correlations along the vertical rungs. This is similar to region II in Fig. 2(d) and Fig. 1 except that the hole and magnon densities are asymmetric across each plaquette. In region V, on the other hand, the hole is trapped in either one of the two plaquettes in a cross-dimer state, similar to region III in Fig. 2, while the other one is spin polarized (see Fig. 7 for the spin correlations). In both cases, S_{total} is reduced by 2.

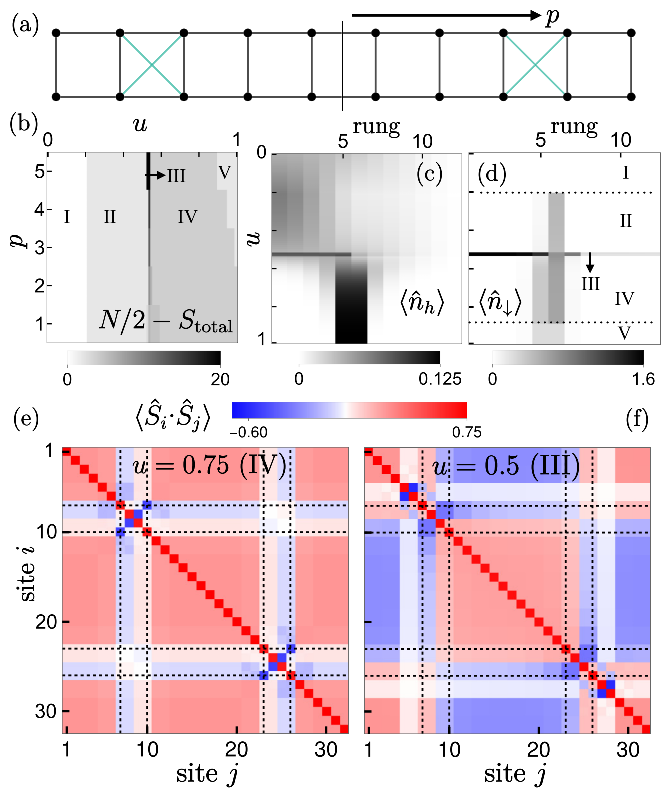

FIG. 3. (a) Ladder with two frustrated plaquettes at a distance p from the center. (b) Phase diagram for $l = 24$, where $N/2 - S_{\text{total}} =$ 2 (II and V), 4 (IV), $\sim\min(4p, 2l - 4p)$ (III). (c) Hole density and (d) magnon density for $l = 24$, $p = 5$. (e) and (f) Spin correlations for $l = 16$, $p = 4$, showing singlet on each diagonal in region IV and two domain walls in region III. Sites are numbered from left to right, with odd integers for the lower leg and even integers for the upper leg, as in Fig. 1(a). The frustrated plaquettes behave collectively in III and IV.

In contrast, regions III and IV represent collective behavior. In region IV, the hole is shared by the two plaquettes, each of which binds two magnons, reducing S_{total} by 4. This state exhibits singlet correlations on the diagonals [Fig. 3(e)], which originates from a cross-dimer on one of the plaquettes and distorted singlets on the other, captured by the variational wave function

$$|\psi(\alpha)\rangle = |\mathbf{x}(\alpha)\rangle \otimes |\times\rangle_\downarrow + |\times\rangle_\downarrow \otimes |\mathbf{x}(\alpha)\rangle. \tag{2}$$

Here, $|\mathbf{x}(\alpha)\rangle$ describes distorted singlets of the form

$$|\mathbf{x}(\alpha)\rangle = (S_2^- - \alpha S_3^-)(S_1^- - \alpha S_4^-)|\uparrow\uparrow\uparrow\uparrow\rangle \tag{3}$$

across the diagonals of a square, where the site numbers refer to those in Fig. 1(a), and $\alpha \sim 0.6$ is the deformation parameter (see Appendix B for details). Crucially, this ordering would not be possible if the plaquettes behaved independently, as there is no reason to bind the distorted singlets in the absence of the hole. Indeed, the state is destabilized by increasing the separation p as the hole gets completely localized on one side [Fig. 3(b)].

Surprisingly, we also find a narrow region (III) close to $u = 0.5$ where S_{total} is very small. Here, the hole is confined in between the two frustrated plaquettes [Fig. 3(c)], and there are

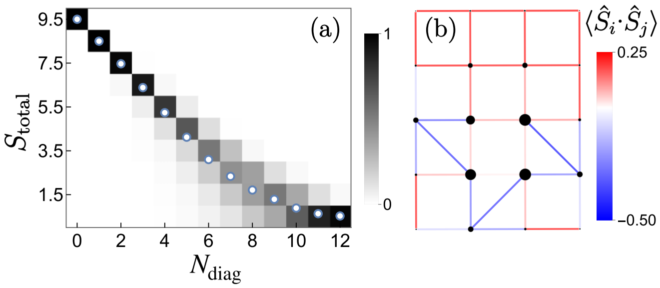

FIG. 4. (a) Reduction of total spin with the number of diagonal bonds in a 4×5 grid, where the bonds are added randomly with at most one per plaquette. Dots show the average values, and gray scale shows the distributions for up to 1000 graphs. Allowing two diagonals per plaquette produces a similar variation. (b) Distribution of the hole, given by the radii of the black dots, and spin correlation on the bonds, given by the color scale, for a sample graph, showing singlets on the diagonals while the other sites are aligned. Generally, correlations between non-neighboring sites (not shown) are weaker.

two domain walls at $\pm p$ separating regions of opposite magnetization [Fig. 3(f)]. We have performed total-spin resolved density matrix renormalization group (DMRG) simulations using the BLOCK2 library [43] to extend the results from exact diagonalization to small values of S_{total}.

The ferromagnetic backgrounds are not affected by system size, and we find the same phase diagram up to $l = 32$. In contrast, for exchange coupling $S_{\text{total}} = 0\ \forall u$, and the plaquettes do not behave collectively (see SM [37]).

Grid with diagonal bonds. To study the effect of building up frustration, we add diagonal bonds to a rectangular grid one at a time, with the same hopping $t > 0$ on all bonds, and study the ground state using exact diagonalization. If the diagonals are drawn at random from a Shastry-Sutherland lattice [44], we find each of them reduces S_{total} by 1. Even if the bonds are drawn without such a constraint, similar behavior is reproduced [Fig. 4(a)]. Based on the collective physics of two plaquettes (region IV in Fig. 3), we expect this reduction arises from the hole being shared by all the diagonals, each of which binds a singlet. Such a structure is supported by the spin correlations [see Fig. 4(b)] and agrees with Ref. [45] for a regular Shastry-Sutherland lattice. As before, we do not expect the physics to be limited by system size.

It is surprising that a local change in topology would alter the collective ordering of a strongly correlated quantum system in such a predictable manner. This does not occur for exchange magnetism, where the diagonal bonds have $\langle \hat{S}_i \cdot \hat{S}_j \rangle > 0$ (see SM [37]).

Random graphs. Finally, we examine whether the role of frustration in shaping the magnetic order extends to random Erdős-Rényi graphs with a given number of sites and bonds. While such graphs do not have well-defined frustration centers, their frustration level can be measured by the number of odd loops or by the frustration index [46–48], which is the minimum number of bonds one has to remove to make the graph bipartite. From exact diagonalization for 20-site graphs (Hilbert-space size $\sim 2 \times 10^6$), we find a strong negative correlation (~ -0.5) between S_{total} and the frustration index (Appendix C). In addition, S_{total} is positively correlated with the numbers of even loops and anticorrelated with the numbers of odd loops [Fig. 5(a)]. In fact, these correlations also persist at the level of individual bonds [Fig. 5(b)], showing the spin alignment across a bond is directly related to how frustrated that bond is (see Appendix C for other measures and SM [37] for other system sizes). The correlations get weaker with increasing loop size as a large loop generically overlaps with many smaller loops.

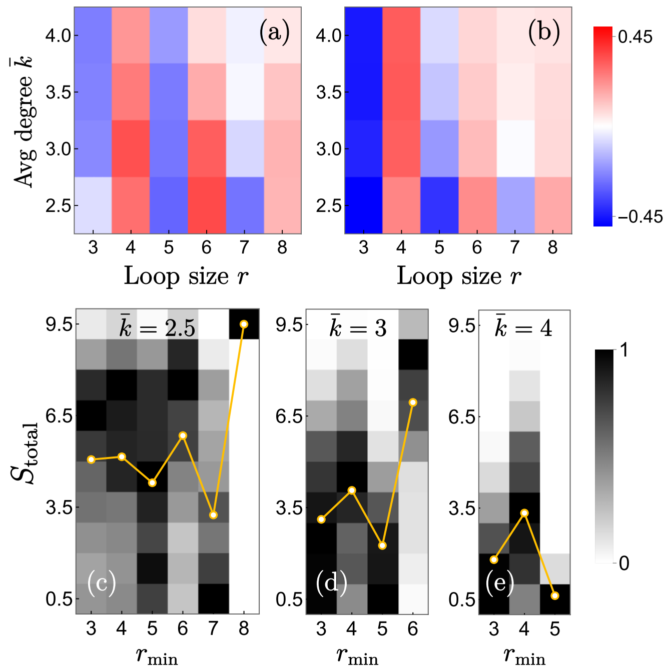

FIG. 5. (a) Correlation between S_{total} and the number of loops of a given size r in 20-site random graphs, where $\bar{k}$ is the average number of neighbors per site. (b) Average correlation between the spin alignment across individual bonds $\langle \hat{S}_i \cdot \hat{S}_j \rangle$ and the number of loops that the bond is a part of, showing that the alignment is strongly governed by local frustration. (c)–(e) Oscillation of the distribution (gray scale) and average value (yellow dots) of S_{total} with the minimum loop size r_{min} in a graph. The statistics for each parameter set are obtained from an ensemble of 1000 nonseparable graphs.

With the above insight, one can tune the magnetization of random graphs by limiting the minimum loop size (girth) r_{min} [49]. As r_{min} is increased, the average value of S_{total} as well as its distribution swings back and forth [Figs. 5(c)–5(e)], moving to higher (lower) values with the removal of odd (even) loops, until one reaches the maximum girth [50]. If this is even, the graphs become close to bipartite and ferromagnetic, whereas if it is odd, they are strongly frustrated with a small S_{total}. None of these variations are present for a Heisenberg model (SM [37]).

Conclusions. In summary, the interplay of strong interactions, kinetic frustration, and nonuniform topology gives rise to the physics of singlet binding, allowing one to shape the magnetic order of strongly correlated fermions by embedding frustration. This is fundamentally different from exchange magnetism and has no classical analog.

While it is challenging to realize Hubbard models with arbitrary connectivity, one can use well-established techniques to locally turn on diagonal hops for cold atoms in optical lattices. Such systems offer a controllable testbed for the Hubbard model [51–53] and was used recently to observe signatures of kinetic magnetism at the single-hole limit with up to $U/t = 72$ [16,17,54]. As we quantify in Appendix D, one can mediate diagonal hops via an intermediate site at the center of the selected plaquette by applying a focused laser beam. The energy scales can be tuned further by modulating [22] or staggering [55] the on-site potentials. More general connectivities should be possible for limited number of sites using digital quantum simulation [56,57] with programmable atom arrays [23] and superconducting qubits [58,59].

Our findings motivate further studies of kinetic magnetism on graphs that can explore (i) deeper connections to polaron physics [42,60] and effective spin models [5,12], (ii) the physics of multiple holes, which is even richer and sensitive to the underlying geometry [42,61–70], (iii) string orders arising from the competition of exchange and kinetic magnetism [42,71–74], (iv) the importance of other graph properties such as separability and heterogeneity [34,35,39,40,75–78], (v) the effect of thermal fluctuations [79–81], and (vi) broader strong-correlation physics of the doped Hubbard model [82] on graphs. More generally, our results show how one can harness quantum effects on networks to control collective behavior, strongly encouraging future studies at the intersection of network science and quantum condensed matter.

Acknowledgments. We thank Alex Wietek, Roderich Moessner, Claudio Castelnovo, Ajit Balram, Kaden Hazzard, Mohit Randeria, and Subhro Bhattacharjee for stimulating discussions. This research was supported by the Anusandhan National Research Foundation (ANRF), India under the Prime Minister Early Career Research Grant (Project No. ANRF/ECRG/2024/005069/PMS).

Data availability. The data and source codes supporting the findings of this study are openly available [83,84].

Appendix A: Square grid with a frustrated plaquette. The ordering of a square grid with a central frustrated plaquette is similar to that of the ladder, as shown in Fig. 6. Compared with the ladder [Figs. 2(b)–2(d)], region II with $(\pm, \mp)$ parity is smaller, and the $\downarrow$-spin density is more delocalized in II and more tightly bound to the center in III. Third-order perturbation in t/t' shows that the latter is described by a 4:1:1 superposition of three cross-dimer states, as sketched in Fig. 6(e): (i) $|\times\rangle_\downarrow$, (ii) $|\times\rangle_{\uparrow,(1,0)}$, where the second $\downarrow$ spin is in the neighboring horizontal plaquettes, and (iii) $|\times\rangle_{\uparrow,(0,1)}$, where it is in the neighboring vertical plaquettes. Thus, the probability of finding a magnon outside the center is $P_{\text{out}} = \frac{1}{9}$, as opposed to $\frac{1}{5}$ for the ladder, which means they are more tightly bound even though there are more ways to delocalize.

Appendix B: Ladder with two frustrated plaquettes. As explained in the main text, two frustrated plaquettes in a ladder behave independently in regions II and V of Fig. 3. Figure 7 shows the spin correlations in these two regions. In II, the hole is delocalized throughout the ladder and each plaquette binds a magnon, leading to singlet correlations along the two vertical rungs that are closer to the boundary. In V, the hole is completely localized in one of the plaquettes which assumes the cross-dimer state $|\times\rangle_\downarrow$, while the other is spin polarized.

In contrast, in region IV the hole is shared by the two plaquettes, each of which binds two magnons [Fig. 3(e)]. This binding can be understood by focusing on the part of the wave function $|\text{GS}'\rangle$ where both the hole and the magnons are contained in the frustrated plaquettes. This is well approximated by the variational form $|\psi(\alpha)\rangle$ in Eqs. (2) and (3). Figure 8 shows that the optimal value α^*, which maximizes the overlap $|\langle\psi(\alpha)|\text{GS}'\rangle|^2$, is close to 0.6 and varies slowly with u.

Appendix C: Random graphs. As shown in Fig. 5, both S_{total} and spin alignment across individual bonds exhibit positive and negative correlations with the numbers of even and odd loops, respectively. Figures 9(a) and 9(b) show that this

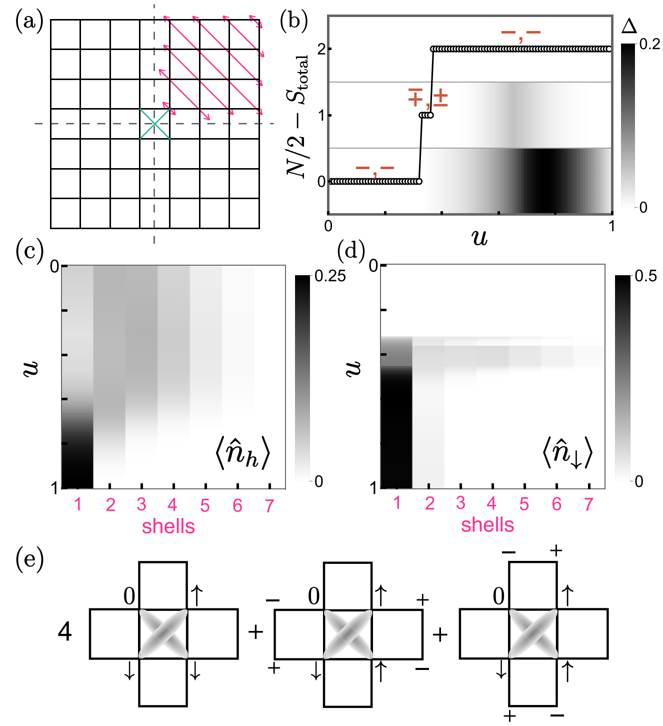

FIG. 6. (a) Square grid with a central frustrated plaquette. The pink arrows define "shells" composed of sites at a given hop distance from the center. (b) Minimum energy sector and ground-state parity, with the gray background showing the excitation gap. (c) Hole occupation and (d) $\downarrow$-spin occupation of different shells. (e) Sketch of the ground state for large u.

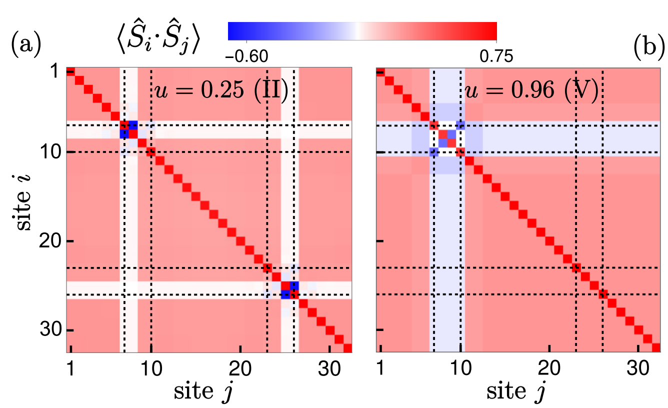

FIG. 7. Spin correlations for a ladder with two frustrated plaquettes, showing one vertical singlet on each in region II and two diagonal singlets on one in region V [cf. Figs. 3(e) and 3(f)].

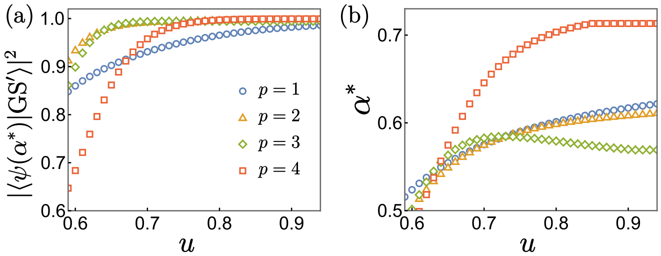

FIG. 8. (a) Maximum overlap $|\langle\psi(\alpha^*)|\mathrm{GS}'\rangle|^2$ and (b) deformation α^* describing singlets in region IV for $l = 10$.

feature is even more prominent in graphs without triangles ($r_{\min} = 4$). In addition, Fig. 9(c) shows a strong negative correlation between S_{total} and the frustration index [46–48], i.e., more nonbipartite graphs have lower net magnetization. No such correlation is found for exchange magnetism [34]. Figure 9(d) shows a similar correlation of the spin alignment across individual bonds with (1) reduction in the frustration index due to removal of that bond and (2) odd/even parity of the smallest loop containing the bond, both of which measure how frustrated the bond is.

Note that the statistics are obtained from nonseparable graphs, for which S_{total} is unique in the ground state [40].

Appendix D: Realizing diagonal hops in an optical lattice. Here, we outline a procedure to realize diagonal hopping in selected plaquettes of a square lattice for ultracold atoms. These atoms are trapped in an optical potential $V(\mathbf{r})$ created by off-resonant laser beams, which produce a dipole force proportional to the laser intensity [85]. Using standing-wave lasers in orthogonal directions yields $V = V_0[\cos^2(\pi x/a) + \cos^2(\pi y/a)] + V_z \cos^2(\pi z/a)$, where a is the lattice spacing. One can freeze the motion along z and confine the x-y dynamics to the lowest energy band by setting $V_z \gg V_0 \gg E_r$, where $E_r := \pi^2\hbar^2/(2ma^2)$ is the recoil energy, and m is the atomic mass. The resulting nearest-neighbor tunneling t_0 decreases sharply with V_0/E_r [86]. Loading fermionic atoms with two hyperfine states realizes a Hubbard model [53], where the interaction U is tunable over a wide range [16,87,88].

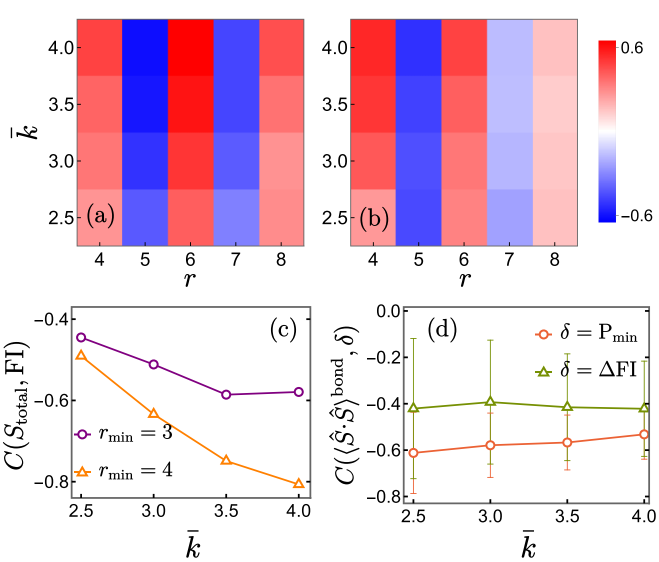

FIG. 9. Correlation of (a) S_{total} and (b) spin alignment across individual bonds with the associated number of loops for 20-site random graphs without triangles ($r_{\min} = 4$) [cf. Figs. 5(a) and 5(b)]. (c) Correlation of S_{total} with the frustration index (FI). (d) Correlation of the spin alignment across a bond with (i) parity $P_{\min}$ (even = 0, odd = 1) of the smallest loop size containing the bond and (ii) change in FI due to removal of that bond, averaged over 1000 random graphs with $r_{\min} = 3$ (dots give mean values and error bars give standard deviations).

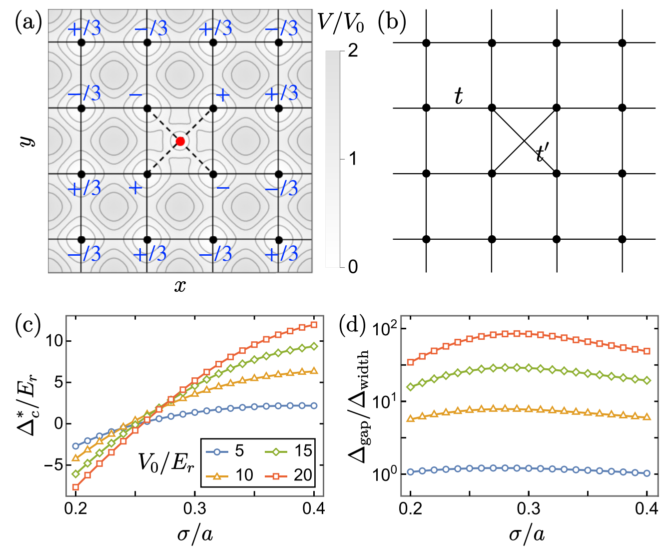

FIG. 10. (a) Square lattice (black dots) with a central site (red dot), generated by the potential $V = V_0[\cos^2(\pi x/a) + \cos^2(\pi y/a)] + (\Delta_c - 2V_0)\exp[-(x^2 + y^2)/\sigma^2]$, with $\Delta_c = 0.04V_0$ and $\sigma = a/4$. The central site mediates diagonal hops (dashed lines). The blue labels represent amplitudes of high-frequency modulation of the on-site potentials to obtain equal hopping on all bonds. (b) Resulting graph with $t' \approx t$. (c) Required offset Δ_c^* for equal hops in units of the recoil energy E_r. (d) Energy gap from the lowest band relative to the band width.

In recent years, it has become possible to engineer the potential landscape within a unit cell using spatial light modulators [21,89–91]. For diagonal hops, one can focus a Gaussian beam at the center of the selected plaquette to create a local minimum with offset Δ_c [Fig. 10(a)]. It is possible to vary Δ_c and the beam width σ such that the Wannier function at the minimum is gapped but mediates a virtual diagonal hopping $t' \sim t_0$ [Figs. 10(c) and 10(d)].

The smaller potential barrier inside the square also increases the hopping $t_\square$ along its edges. To rectify this distortion, one can either apply additional repulsive potentials on the edges or, following Ref. [22], modulate the on-site potentials with amplitude $\pm A$ on the square and $\pm A/3$ outside, as sketched in Fig. 10(a). For high modulation frequency ω, such driving rescales the nondiagonal hops to $t_\square J_0(\frac{2A}{\omega})$ and $t_0 J_0(\frac{2A}{3\omega})$, where J_0 is the Bessel function of the first kind. Thus, all bonds have equal hopping if $t' = t_\square J_0(\frac{2A}{\omega}) = t_0 J_0(\frac{2A}{3\omega})$. Figures 10(c) and 10(d) show this condition can be met while maintaining a large gap for a range of Gaussian beams and $V_0/E_r \gtrsim 5$. The hopping is close to t_0 and decreases slowly with σ.

Note that the procedure can be readily generalized for multiple frustrated plaquettes.

[1] Edited by C. Lacroix, P. Mendels, and F. Mila, in *Introduction to Frustrated Magnetism: Materials, Experiments, Theory* (Springer, New York, 2011), Vol. 164.

[2] Edited by H. T. Diep, *Frustrated Spin Systems* (World Scientific, Singapore, 2013).

[3] L. Balents, Spin liquids in frustrated magnets, Nature (London) **464**, 199 (2010).

[4] R. Moessner and A. P. Ramirez, Geometrical frustration, Phys. Today **59**(2), 24 (2006).

[5] J. O. Haerter and B. S. Shastry, Kinetic antiferromagnetism in the triangular lattice, Phys. Rev. Lett. **95**, 087202 (2005).

[6] D. C. Mattis, *The Theory of Magnetism I: Statics and Dynamics* (Springer, Berlin, 1981), p. 258.

[7] J. Keeling, *Quantum Magnetism*, Lecture Notes (University of St. Andrews, 2008).

[8] H. Tasaki, *Physics and Mathematics of Quantum Many-Body Systems* (Springer, Cham, 2020).

[9] D. P. Arovas, E. Berg, S. A. Kivelson, and S. Raghu, The Hubbard model, Annu. Rev. Condens. Matter Phys. **13**, 239 (2022).

[10] Y. Nagaoka, Ferromagnetism in a narrow, almost half-filled s band, Phys. Rev. **147**, 392 (1966).

[11] K.-S. Kim, Exact hole-induced resonating-valence-bond ground state in certain $U = \infty$ Hubbard models, Phys. Rev. B **107**, L140401 (2023).

[12] C. N. Sposetti, B. Bravo, A. E. Trumper, C. J. Gazza, and L. O. Manuel, Classical antiferromagnetism in kinetically frustrated electronic models, Phys. Rev. Lett. **112**, 187204 (2014).

[13] C. Glittum, A. Štrkalj, D. Prabhakaran, P. A. Goddard, C. D. Batista, and C. Castelnovo, A resonant valence bond spin liquid in the dilute limit of doped frustrated Mott insulators, Nat. Phys. **21**, 1211 (2025).

[14] D. Poilblanc, Enhanced pairing in doped quantum magnets with frustrated hole motion, Phys. Rev. Lett. **93**, 197204 (2004).

[15] J. P. Dehollain, U. Mukhopadhyay, V. P. Michal, Y. Wang, B. Wunsch, C. Reichl, W. Wegscheider, M. S. Rudner, E. Demler, and L. M. K. Vandersypen, Nagaoka ferromagnetism observed in a quantum dot plaquette, Nature (London) **579**, 528 (2020).

[16] M. Lebrat, M. Xu, L. H. Kendrick, A. Kale, Y. Gang, P. Seetharaman, I. Morera, E. Khatami, E. Demler, and M. Greiner, Observation of Nagaoka polarons in a Fermi-Hubbard quantum simulator, Nature (London) **629**, 317 (2024).

[17] M. L. Prichard, B. M. Spar, I. Morera, E. Demler, Z. Z. Yan, and W. S. Bakr, Directly imaging spin polarons in a kinetically frustrated Hubbard system, Nature (London) **629**, 323 (2024).

[18] T. Hanisch, B. Kleine, A. Ritzl, and E. Müller-Hartmann, Ferromagnetism in the Hubbard model: Instability of the Nagaoka state on the triangular, honeycomb and kagome lattices, Ann. Phys. (NY) **507**, 303 (1995).

[19] F. T. Lisandrini, B. Bravo, A. E. Trumper, L. O. Manuel, and C. J. Gazza, Evolution of Nagaoka phase with kinetic energy frustrating hopping, Phys. Rev. B **95**, 195103 (2017).

[20] D. Buterakos and S. Das Sarma, Ferromagnetism in quantum dot plaquettes, Phys. Rev. B **100**, 224421 (2019).

[21] C. Gross and W. S. Bakr, Quantum gas microscopy for single atom and spin detection, Nat. Phys. **17**, 1316 (2021).

[22] G. M. Nixon, F. N. Ünal, and U. Schneider, Individually tunable tunnelling coefficients in optical lattices using local periodic driving, Quantum Sci. Technol. **9**, 045030 (2024).

[23] D. González-Cuadra, D. Bluvstein, M. Kalinowski, R. Kaubruegger, N. Maskara, P. Naldesi, T. V. Zache, A. M. Kaufman, M. D. Lukin, H. Pichler, *et al.*, Fermionic quantum processing with programmable neutral atom arrays, Proc. Natl. Acad. Sci. USA **120**, e2304294120 (2023).

[24] S. B. Bravyi and A. Y. Kitaev, Fermionic quantum computation, Ann. Phys. (NY) **298**, 210 (2002).

[25] F. Verstraete and J. I. Cirac, Mapping local Hamiltonians of fermions to local Hamiltonians of spins, J. Stat. Mech. (2005) P09012.

[26] M. Steudtner and S. Wehner, Quantum codes for quantum simulation of fermions on a square lattice of qubits, Phys. Rev. A **99**, 022308 (2019).

[27] S. H. Strogatz, Exploring complex networks, Nature (London) **410**, 268 (2001).

[28] M. E. J. Newman, *Networks: An Introduction* (Oxford University Press, Oxford, 2018).

[29] A. Barrat, M. Barthelemy, and A. Vespignani, *Dynamical Processes on Complex Networks* (Cambridge University Press, Cambridge, 2008).

[30] S. N. Dorogovtsev, A. V. Goltsev, and J. F. F. Mendes, Critical phenomena in complex networks, Rev. Mod. Phys. **80**, 1275 (2008).

[31] R. M. D'Souza, J. Gómez-Gardeñes, J. Nagler, and A. Arenas, Explosive phenomena in complex networks, Adv. Phys. **68**, 123 (2019).

[32] J. Nokkala, J. Piilo, and G. Bianconi, Complex quantum networks: A topical review, J. Phys. A: Math. Theor. **57**, 233001 (2024).

[33] A. Grabarits, K. R. Swain, M. S. Heydari, P. Chandarana, F. J. Gómez-Ruiz, and A. del Campo, Quantum chaos in random Ising networks, Phys. Rev. Res. **7**, 013146 (2025).

[34] P. Gopalakrishnan and S. Dutta, Frustrated quantum magnetism on complex networks: What sets the total spin, arXiv:2403.09116.

[35] Y. Horiike and Y. Kawaguchi, A comprehensive exploration of interaction networks reveals a connection between entanglement and network structure, arXiv:2505.11466.

[36] X. Zheng, D. Zeng, and F.-Y. Wang, Social balance in signed networks, Inf. Syst. Front. **17**, 1077 (2015).

[37] See Supplemental Material at https://link.aps.org/supplemental/10.1103/stj9-srp1 for comparisons with Heisenberg antiferromagnetism and data for random graphs of varying system size, which includes Refs. [92,93].

[38] F. H. Essler, H. Frahm, F. Göhmann, A. Klümper, and V. E. Korepin, *The One-Dimensional Hubbard Model* (Cambridge University Press, Cambridge, 2005).

[39] H. Tasaki, Extension of Nagaoka's theorem on the large-U Hubbard model, Phys. Rev. B **40**, 9192 (1989).

[40] E. Bobrow, K. Stubis, and Y. Li, Exact results on itinerant ferromagnetism and the 15-puzzle problem, Phys. Rev. B **98**, 180101(R) (2018).

[41] B. J. Powell, Balance and frustration in strongly correlated itinerant electron systems: An extension of Nagaoka's theorem, Phys. Rev. B **96**, 174435 (2017).

[42] I. Morera, A. Bohrdt, W. W. Ho, and E. Demler, Attraction from kinetic frustration in ladder systems, Phys. Rev. Res. **6**, 023196 (2024).

[43] H. Zhai, H. R. Larsson, S. Lee, Z.-H. Cui, T. Zhu, C. Sun, L. Peng, R. Peng, K. Liao, J. Tölle, *et al.*, BLOCK2: A

comprehensive open source framework to develop and apply state-of-the-art DMRG algorithms in electronic structure and beyond, J. Chem. Phys. **159**, 234801 (2023).

[44] B. S. Shastry and B. Sutherland, Exact ground state of a quantum mechanical antiferromagnet, Physica B+C **108**, 1069 (1981).

[45] P. W. Leung and Y. F. Cheng, Absence of hole pairing in a simple t-J model on the Shastry-Sutherland lattice, Phys. Rev. B **69**, 180403(R) (2004).

[46] P. Holme, F. Liljeros, C. R. Edling, and B. J. Kim, Network bipartivity, Phys. Rev. E **68**, 056107 (2003).

[47] S. Aref and M. C. Wilson, Measuring partial balance in signed networks, J. Complex Netw. **6**, 566 (2018).

[48] S. Aref and M. C. Wilson, Balance and frustration in signed networks, J. Complex Netw. **7**, 163 (2019).

[49] M. Bayati, A. Montanari, and A. Saberi, Generating random networks without short cycles, Oper. Res. **66**, 1227 (2018).

[50] J. Verstraëte, Extremal problems for cycles in graphs, in *Recent Trends in Combinatorics* (Springer, Cham, 2016), p. 83.

[51] T. Esslinger, Fermi-Hubbard physics with atoms in an optical lattice, Annu. Rev. Condens. Matter Phys. **1**, 129 (2010).

[52] C. Gross and I. Bloch, Quantum simulations with ultracold atoms in optical lattices, Science **357**, 995 (2017).

[53] L. Tarruell and L. Sanchez-Palencia, Quantum simulation of the Hubbard model with ultracold fermions in optical lattices, C. R. Phys. **19**, 365 (2018).

[54] G. Ji, M. Xu, L. H. Kendrick, C. S. Chiu, J. C. Brüggenjürgen, D. Greif, A. Bohrdt, F. Grusdt, E. Demler, M. Lebrat, *et al.*, Coupling a mobile hole to an antiferromagnetic spin background: Transient dynamics of a magnetic polaron, Phys. Rev. X **11**, 021022 (2021).

[55] T. Chalopin, P. Bojović, D. Bourgund, S. Wang, T. Franz, I. Bloch, and T. Hilker, Optical superlattice for engineering Hubbard couplings in quantum simulation, Phys. Rev. Lett. **134**, 053402 (2025).

[56] S. Lloyd, Universal quantum simulators, Science **273**, 1073 (1996).

[57] L. B. Oftelie, M. Urbanek, M. Metcalf, J. Carter, A. F. Kemper, and W. A. de Jong, Simulating quantum materials with digital quantum computers, Quantum Sci. Technol. **6**, 043002 (2021).

[58] R. Barends *et al.*, Digital quantum simulation of fermionic models with a superconducting circuit, Nat. Commun. **6**, 7654 (2015).

[59] L. Lamata, A. Parra-Rodriguez, M. Sanz, and E. Solano, Digital-analog quantum simulations with superconducting circuits, Adv. Phys.: X **3**, 1457981 (2018).

[60] R. Samajdar and R. N. Bhatt, Polaronic mechanism of Nagaoka ferromagnetism in Hubbard models, Phys. Rev. B **109**, 235128 (2024).

[61] B. Doucot and X. G. Wen, Instability of the Nagaoka state with more than one hole, Phys. Rev. B **40**, 2719 (1989).

[62] B. S. Shastry, H. R. Krishnamurthy, and P. W. Anderson, Instability of the Nagaoka ferromagnetic state of the $U = \infty$ Hubbard model, Phys. Rev. B **41**, 2375 (1990).

[63] J. A. Riera and A. P. Young, Ferromagnetism in the one-band Hubbard model, Phys. Rev. B **40**, 5285 (1989).

[64] I. Ivantsov, A. Ferraz, and E. Kochetov, Breakdown of the Nagaoka phase at finite doping, Phys. Rev. B **95**, 155115 (2017).

[65] H. B. Xavier, E. Kochetov, and A. Ferraz, Onset of ferromagnetism for strongly correlated electrons in one-dimensional chains, Phys. Rev. B **101**, 045112 (2020).

[66] S.-S. Zhang, W. Zhu, and C. D. Batista, Pairing from strong repulsion in triangular lattice Hubbard model, Phys. Rev. B **97**, 140507(R) (2018).

[67] S. Yun, W. Dobrautz, H. Luo, V. Katukuri, N. Liebermann, and A. Alavi, Ferromagnetic domains in the large-U Hubbard model with a few holes: A full configuration interaction quantum Monte Carlo study, Phys. Rev. B **107**, 064405 (2023).

[68] L. Liu, H. Yao, E. Berg, S. R. White, and S. A. Kivelson, Phases of the infinite U Hubbard model on square lattices, Phys. Rev. Lett. **108**, 126406 (2012).

[69] Z. Zhu, D. N. Sheng, and A. Vishwanath, Doped Mott insulators in the triangular-lattice Hubbard model, Phys. Rev. B **105**, 205110 (2022).

[70] P. Sharma, Y. Peng, D. N. Sheng, H. J. Changlani, and Y. Wang, Instability of Nagaoka state and quantum phase transition via kinetic frustration control, Phys. Rev. Res. **8**, 023070 (2026).

[71] P. Béran, D. Poilblanc, and R. Laughlin, Evidence for composite nature of quasiparticles in the 2D t-J model, Nucl. Phys. B **473**, 707 (1996).

[72] C. S. Chiu, G. Ji, A. Bohrdt, M. Xu, M. Knap, E. Demler, F. Grusdt, M. Greiner, and D. Greif, String patterns in the doped Hubbard model, Science **365**, 251 (2019).

[73] F. Grusdt, A. Bohrdt, and E. Demler, Microscopic spinon-chargon theory of magnetic polarons in the t-J model, Phys. Rev. B **99**, 224422 (2019).

[74] H. Schlömer, U. Schollwöck, A. Bohrdt, and F. Grusdt, Kinetic-to-magnetic frustration crossover and linear confinement in the doped triangular t-J model, Phys. Rev. B **110**, L041117 (2024).

[75] Y. Watanabe and S. Miyashita, Existence of saturated ferromagnetic and spiral states in 1D Lieb-ferrimagnetic models away from half-filling, J. Phys. Soc. Jpn. **68**, 3086 (1999).

[76] Y. Li, K. Liu, and G. W. Bryant, Nagaoka ferromagnetism in 3×3 arrays and beyond, Phys. Rev. B **110**, 245141 (2024).

[77] A. Mielke, Ferromagnetism in the Hubbard model on line graphs and further considerations, J. Phys. A: Math. Gen. **24**, 3311 (1991).

[78] N. Hernandez-Cepeda and S. E. Ulloa, Optimal array geometries for kinetic magnetism and Nagaoka polarons, Phys. Rev. B **113**, 075156 (2026).

[79] I. Morera, M. Kanász-Nagy, T. Smolenski, L. Ciorciaro, A. Imamoğlu, and E. Demler, High-temperature kinetic magnetism in triangular lattices, Phys. Rev. Res. **5**, L022048 (2023).

[80] R. C. Newby and E. Khatami, Finite-temperature kinetic ferromagnetism in the square-lattice Hubbard model, Phys. Rev. B **111**, 245120 (2025).

[81] D. Pereira and E. J. Mueller, Kinetic magnetism in the crossover between the square and triangular lattice Fermi-Hubbard models, Phys. Rev. B **112**, 245120 (2025).

[82] P. A. Lee, N. Nagaosa, and X.-G. Wen, Doping a Mott insulator: Physics of high-temperature superconductivity, Rev. Mod. Phys. **78**, 17 (2006).

[83] R. B. S and S. Dutta, Dataset for "Shaping magnetic order by local frustration for itinerant fermions on a graph", Zenodo, 2026, http://doi.org/10.5281/zenodo.19019802.

[84] R. B. S and S. Dutta, Source codes for "Shaping magnetic order by local frustration for itinerant fermions on a graph", Zenodo, 2026, http://doi.org/10.5281/zenodo.19028546.

[85] R. Grimm, M. Weidemüller, and Y. B. Ovchinnikov, Optical dipole traps for neutral atoms, Adv. At. Mol. Opt. Phys. **42**, 95 (2000).

[86] I. Bloch and M. Greiner, Exploring quantum matter with ultracold atoms in optical lattices, Adv. At. Mol. Opt. Phys. **52**, 1 (2005).

[87] I. Bloch, J. Dalibard, and W. Zwerger, Many-body physics with ultracold gases, Rev. Mod. Phys. **80**, 885 (2008).

[88] C. Chin, R. Grimm, P. Julienne, and E. Tiesinga, Feshbach resonances in ultracold gases, Rev. Mod. Phys. **82**, 1225 (2010).

[89] C. Weitenberg, M. Endres, J. F. Sherson, M. Cheneau, P. Schauß, T. Fukuhara, I. Bloch, and S. Kuhr, Single-spin addressing in an atomic Mott insulator, Nature (London) **471**, 319 (2011).

[90] P. Zupancic, P. M. Preiss, R. Ma, A. Lukin, M. E. Tai, M. Rispoli, R. Islam, and M. Greiner, Ultra-precise holographic beam shaping for microscopic quantum control, Opt. Express **24**, 13881 (2016).

[91] M. Lebrat, A. Kale, L. H. Kendrick, M. Xu, Y. Gang, A. Nikolaenko, P. M. Bonetti, S. Sachdev, and M. Greiner, Ferrimagnetism of ultracold fermions in a multiband Hubbard system, Science **392**, 612 (2026).

[92] M. Kawamura, K. Yoshimi, T. Misawa, Y. Yamaji, S. Todo, and N. Kawashima, Quantum lattice model solver $\mathcal{H}\Phi$, Comput. Phys. Commun. **217**, 180 (2017).

[93] K. Ido, M. Kawamura, Y. Motoyama, K. Yoshimi, Y. Yamaji, S. Todo, N. Kawashima, and T. Misawa, Update of $\mathcal{H}\Phi$: Newly added functions and methods in versions 2 and 3, Comput. Phys. Commun. **298**, 109093 (2024).